UNIVERSITY OF LEEDS

This is a repository copy of *Contact mechanics and lubrication analyses of ceramic-on-metal total hip replacements*.

White Rose Research Online URL for this paper:
http://eprints.whiterose.ac.uk/74977/

Article:

Meng, Q, Liu, F, Fisher, J et al. (1 more author) (2013) Contact mechanics and lubrication analyses of ceramic-on-metal total hip replacements. Tribology International, 63. 51 - 60. ISSN 0301-679X

https://doi.org/10.1016/j.triboint.2012.02.012

© 2012, Elsevier. Licensed under the Creative Commons Attribution-NonCommercial-NoDerivatives 4.0 International
http://creativecommons.org/licenses/by-nc-nd/4.0/

Reuse

Unless indicated otherwise, fulltext items are protected by copyright with all rights reserved. The copyright exception in section 29 of the Copyright, Designs and Patents Act 1988 allows the making of a single copy solely for the purpose of non-commercial research or private study within the limits of fair dealing. The publisher or other rights-holder may allow further reproduction and re-use of this version - refer to the White Rose Research Online record for this item. Where records identify the publisher as the copyright holder, users can verify any specific terms of use on the publisher's website.

Takedown

If you consider content in White Rose Research Online to be in breach of UK law, please notify us by emailing eprints@whiterose.ac.uk including the URL of the record and the reason for the withdrawal request.

White Rose
university consortium
Universities of Leeds, Sheffield & York

eprints@whiterose.ac.uk
https://eprints.whiterose.ac.uk/

Contact mechanics and lubrication analyses of ceramic-on-metal total hip replacements

Qingen Meng[a, *], Feng Liu[a], John Fisher[a], Zhongmin Jin[a, b]

[a] Institute of Medical and Biological Engineering,

School of Mechanical Engineering,

University of Leeds, UK

[b] School of Mechanical Engineering,

Xi'an Jiaotong University, China

[*] Corresponding author

Tel: 44 113 343 5011

Fax: 44 113 242 4611

Email: Q.Meng@ leeds.ac.uk

Abstract:

Ceramic-on-metal (CoM) total hip replacements have shown reduced wear and friction. Lubrication and contact mechanics analyses play an important role in providing an overall understanding for the tribological performance of CoM bearings. In the present study, the steady-state contact mechanics and elastohydrodynamic lubrication (EHL) and transient EHL of CoM bearings were analysed. The dry and lubricated contact pressures of CoM bearings showed typical characteristics of hard-on-hard hip bearings. The effects of head radius and radial clearance on the lubrication performance were predicted. CoC and CoM bearings are more likely to benefit full fluid film lubrication than MoM bearings.

Keywords: Contact mechanics, Lubrication, Total hip replacement (THR), Ceramic-on-metal (CoM)

1. Introduction

Metal-on-metal (MoM) bearings made from high-carbon cobalt-chromium (CoCr) alloys have been used for both conventional total hip replacement (THR) and surface replacement in recent years due to reduced volumetric wear and larger bearing size giving improved stability. However, the potential long-term effects of elevated levels of metal ions have remained a concern [1-3] along with the very high failure rates that have been reported for one type of MoM resurfacing implant [4]. A new bearing couple, ceramic-on-metal (CoM), consisting of a ceramic head articulating against a metal acetabular liner, has been shown to reduce wear and friction compared to MoM bearings *in vitro* [5-9]. Moreover, a blood metal ion levels measurement indicated that the chromium levels were significantly lower in CoM than in MoM bearings *in vivo* [10]. Recent studies showed that an increase in the size of ceramic head may reduce wear further [11-13]. Therefore, CoM bearing couple is a promising novel design for hip implants and it has been approved recently by The United States Food and Drug Administration [14].

Improved lubrication may be an important reason for the lower wear of CoM bearings, since an effective lubricant film between the bearing surfaces can sustain the applied load while avoids direct asperity contacts. The heavy loads and low entrainment velocities experienced by hip implants result in a fluid film pressure distribution that is very close to the dry (unlubricated) contact pressure. Under adverse conditions, such as when the entrainment velocities approach zero and/or the load are very high, lubricant film may break down. Load is consequently sustained by the direct contact of bearing surfaces. Therefore, both dry contact mechanics and lubrication analyses are important for CoM hip bearings. Computational modelling of lubrication and dry contact mechanics of hip replacements can provide detailed information not only for the pressure distribution and lubricant film thickness in contact area, but also for how design and manufacturing parameters and operating conditions affect the lubrication performance. This information is imperative for further insights into the failure of lubricating film, wear generation and design optimization of hip implants, especially for a newly-developed design like CoM hip bearing.

However, no dry contact mechanics studies have been reported for this promising bearing couple. Moreover, the reported theoretical estimations of the lubrication film of CoM hip bearings were all simply based on a Hamrock-Dowson (H-D) formula [7, 15, 16], which can only calculate the minimum film thickness under steady-state conditions. Therefore, the aim of this study was to analyze the contact mechanics and lubrication of CoM hip bearings using numerical methods. The steady-state contact mechanics and elastohydrodynamic lubrication (EHL) and the transient EHL of CoM hip bearings were solved; the effects of geometric parameters of CoM hip bearings on the contact mechanics and lubrication performance were investigated; and the lubrication performances of MoM, CoM and ceramic-on-ceramic (CoC) hip bearings were compared.

2. Materials and methods

2.1 Materials

A typical CoM THR bearing normally consists of three components, a titanium acetabular shell, a CoCr insert and a ceramic (typically, alumina or alumina matrix composite) head. The CoCr insert is fixed in the titanium acetabular shell using a taper locking mechanism. The acetabular shell is fixed in the acetabulum using a cementless method. The initial stability of the acetabular shell is achieved by screws or spikes while the long term fixation is reached by the in-growth of bone onto and around the porous-coated shell surface. The spherical ceramic head articulates against the hemi-spherical inner surface of the CoCr insert to form a joint. In the present study, the taper lock between the insert and the shell was not modelled and thus a secure locking between the insert and shell was assumed. A uniform thickness of 10 mm and 4 mm was adopted for the CoCr insert and the titanium shell, respectively. The bone and the fixation of the shell were represented by an equivalent support layer with a thickness of 2 mm and appropriate material properties [17]. Such a CoM bearing configuration is shown in Figure 1. All the materials were assumed to be homogeneous and linear elastic. The material properties adopted in the present study are summarized in Table 1. Five CoM THRs with different sizes or radial clearances were analysed in the present study. For the same radial clearance of 60 μm, three commonly used head radii (14 mm, 16 mm and 18 mm) were investigated. For the radius of 18 mm, radial clearances of 30 μm and 100 μm were also simulated. The study assumed correct alignment between the centre of the cup and centre of the head and theoretical alignment of the acetabular cup and head, such that the contact patch on the head did not intersect the rim of the cup.

In order to compare the lubrication performance of the CoM hip bearing with those of the CoC and MoM bearings, the transient EHL of a CoC THR and a MoM THR, both with the head radius of 18 mm and the radial clearance of 60 μm, were also modelled. The head of the simulated CoC hip bearing was similar to the CoM bearings, while an alumina insert was used for the acetabular component of the CoC bearing. The structure of the acetabular component of the investigated MoM bearing was similar to the CoM bearings. However, the head of the MoM bearing was made of CoCr alloy.

2.2 Models

Both steady-state and transient conditions were considered for the EHL models. For the dry contact mechanics models, only the loads used in the steady-state EHL models were imposed. The ball-in-socket geometry shown in Figure 1 was used to study the dry contact mechanics and EHL of CoM hip bearings. Since the inclination of the cup has a negligible effect on the EHL of hip implants provided the contact area is within the cup [18], the cup was positioned horizontally instead of anatomically with an angle of 45°. In reality, both the load and velocity experienced in human hip joints are three-dimensional (3D) and time-dependent [19]. Since the major velocity component of hip implants is in the flexion/extension direction and the resultant load is in the direction of about 10° medially to the vertical axis [19], it was possible to approximate the conditions with an estimated small loss in accuracy by considering only the flexion/extension velocity and vertical component of the load. In steady-state EHL studies, the angular velocity around the z axis was adopted as 2 rad/s [17, 20]. The vertical load was chosen as 3000 N to represent approximately 4 times normal body weight. In the transient analyses, the walking conditions based on the ISO 14242-1 testing standard [21] (Figure 2) were adopted.

The lubricant in artificial hip joints is periprosthetic synovial fluid, which behaves as a powerful non-Newtonian fluid under relatively low shear rates. However, under higher shear rates likely to be experienced in the hip joint (10^5/s), it was considered reasonable to assume the periprosthetic synovial fluid as Newtonian, isoviscous and incompressible [20, 22-24]. A realistic viscosity of 0.002 Pa s was adopted for the synovial fluid in the present study [23].

The governing equations for EHL models were established in spherical coordinates defined in Figure 3. The Reynolds equation for the fluid flow between the bearing surfaces was

$$\sin\theta \frac{\partial}{\partial\theta}\left(h^3 \sin\theta \frac{\partial p}{\partial\theta}\right) + \frac{\partial}{\partial\phi}\left(h^3 \frac{\partial p}{\partial\phi}\right) = 6\eta R_{\mathrm{h}}^2 \sin^2\theta \left(\omega \frac{\partial h}{\partial\phi} + 2\Gamma \frac{\partial h}{\partial t}\right) \tag{1}$$

where p is film pressure; h is film thickness; η is the viscosity of the periprosthetic synovial fluid; t is time; ω is the angular velocity of femoral head; ϕ and θ are spherical coordinates defined in Figure 3. The Γ parameter plays the role of a switch, which could be one or zero to represent a transient or steady-state problem, respectively.

Boundary conditions for the Reynolds equation were

$$p(0,\theta) = p(\pi,\theta) = p(\phi,0) = p(\phi,\pi) = 0$$

$$\partial p/\partial\phi = \partial p/\partial\theta = 0 \tag{2}$$

The film thickness consisted of the undeformed gap and the elastic deformation of bearing surfaces due to the film pressure:

$$h = c - e_x \sin\theta\cos\phi - e_y \sin\theta\sin\phi + \delta \tag{3}$$

where c is the radial clearance between the insert and the head ($c = R_{\mathrm{c}} - R_{\mathrm{h}}$; R_{c} and R_{h} are the radii of the insert and the head, respectively); e_x and e_y are eccentricities of the femoral head; δ is the elastic deformation of bearing surfaces, determined by the deformation coefficients of the bearing surfaces and the film pressure.

In addition, the external load components were balanced by the integration of the film pressure:

$$f_x = R_{\mathrm{h}}^2 \int_0^{\pi}\int_0^{\pi} p \sin^2\theta \cos\phi \, d\theta \, d\phi = 0$$

$$f_y = R_{\mathrm{h}}^2 \int_0^{\pi}\int_0^{\pi} p \sin^2\theta \sin\phi \, d\theta \, d\phi = w_y$$

$$f_z = R_{\mathrm{h}}^2 \int_0^{\pi}\int_0^{\pi} p \sin\theta \cos\theta \, d\theta \, d\phi = 0 \tag{4}$$

2.3 Methods

2.3.1 Dry contact mechanics

3D finite-element (FE) models incorporating the acetabular insert, titanium shell, equivalent support layer and femoral head were created in NX I-DEAS (Version 6.1, Siemens PLM Software Inc., Plano, USA) and solved using ABAQUS (version 6.9-EF1, Dassault Systèmes Simulia Corp., Providence, United States). A mesh convergence study was performed for the bearing with the radius of 18 mm and clearance of 60 µm to determine a proper mesh density. An increase of mesh density from 96 × 96 elements to 128 × 128 elements on the contact surface did not generate appreciable differences in the profile of contact pressure distribution. The differences in the maximum pressure and contact area caused by the two mesh densities were only 0.05 percent and 6 percent, respectively. Therefore, the mesh density of 96 × 96 elements on the contact surface was employed for all the cases, resulting in a total of approximately 129,000 8-node linear brick and 6-node linear triangular prism elements for each dry contact model.

The element-based surfaces of the insert and head were defined as a contact pair, with the insert surface being chosen as the slave surface. “Node to surface” contact discretization was used for the contact pair. “Small sliding” was used as the contact tracking approach. The option of “adjust = 0.0” was adopted to avoid the initial overclosure. The parameter “CLEARANCE”, able to define initial clearance values precisely at slave nodes, was used to accurately specify the initial gap between the bearing surfaces.

The dry contact mechanics of CoM THRs was also calculated using Hertz contact theory, based on the assumption of semi-infinite solids for the ceramic and metal bearing surfaces. This was done by means of an equivalent ball-on-plane model. The radius of the equivalent ball, R, was determined from the radii of the insert and head, R_c and R_h, and the radial clearance, c:

$$R = \frac{R_c R_h}{c} \tag{5}$$

This enabled the contact radius, r, and the maximum contact pressure, p_{max}, to be determined under given load, w:

$$r = \left(\frac{3wR}{E'} \right)^{1/3} \tag{6}$$

$$p_{max} = \frac{3w}{2\pi r^2} \tag{7}$$

where E' is the equivalent elastic modulus of the ceramic and metal bearing surfaces, determined by the elastic moduli and Poisson's rations of the CoCr insert and the ceramic head, E_c ν_c, E_h and ν_h:

$$\frac{1}{E'} = \frac{1}{2}\left(\frac{1-\nu_c{}^2}{E_c} + \frac{1-\nu_h{}^2}{E_h} \right) \tag{8}$$

2.3.2. Elastohydrodynamic lubrication

Found Briefly, for a steady-state problem, the governing equations were non-dimensionalised to facilitate the numerical analysis and improve the stability of the numerical process; the Reynolds equation was solved using a multi-grid method; while the elastic deformation was calculated using a multi-level multi-integration technique [27, 28]. The load balance was satisfied through adjusting the eccentricities of the head according to the calculated load components from the film pressure. Three levels of grid were used in the multilevel solver. On the finest level, 257 nodes were arranged in both the θ and ϕ directions [18, 29]. For the transient models, the walking cycle was divided into 100 time steps (200 time steps made negligible difference in solutions from 100 time steps). At each time step, the numerical procedure was similar to that of a steady-state problem. The simulation of a transient model started with a steady-state solution. The convergent solutions for film thickness, pressure and eccentricities at one time step were used as initial values for the next time step until four walking cycles were finished, when the cyclic convergence had been achieved.

The deformation coefficients used to calculate the elastic deformation of the bearing surfaces were calculated using a FE-based method [30]. In brief, FE models were created for cups and heads. A unit pressure was applied to an element located at the centre of the articulating surface of the insert or the head. The displacement distribution along a longitudinal line caused by the unit pressure was calculated using ABAQUS. These displacement coefficients were used to curve fit a displacement influence function making use of spherical distance as the independent variable. The coefficients at each node were subsequently calculated using the curve-fitted function.

3. Results

Figure 4 shows the contour plots of dry contact pressure distribution at the bearing surface for different R_h, with the same radial clearance of 60 μm. The contour plots of dry contact pressure distribution at the bearing surface for different radial clearances, with the same radius of 18 mm are plotted in Figure 5. For all the cases considered in the present study for the dry contact mechanics of CoM bearings, the maximum contact pressures and contact areas predicted from the FE method and the Hertz contact theory are listed in Table 2. The contour plots of film pressure predicted by steady-state EHL for different radii with the same radial clearance are shown in Figure 6. Figure 7 shows the contour plots of film pressure predicted by steady-state EHL for different radial clearances with a fixed R_h of 18 mm. In Figure 8, the minimum film thickness predicted from the present steady-state EHL model of a CoM THR (R_h = 18 mm, c = 60 μm) is compared with that calculated from the H-D formula [31, 32], which is as follows

$$\frac{h_{\min}}{R} = 2.80 \times \left(\frac{\eta u}{E'R}\right)^{0.65} \left(\frac{w}{E'R^2}\right)^{-0.21} \tag{9}$$

where u is the effective entraining velocity, calculated from $u = \omega R_h/2$ for the present problem. Figure 9 shows the effects of radius and radial clearance on the steady-state film thickness along the central line in the entraining direction. Figure 10 compares the central and minimum film thicknesses and the maximum pressure between CoM THRs with different radii but a similar radial clearance, predicted from transient EHL models. The central and minimum film thicknesses and the maximum pressure predicted from transient EHL models for CoM THRs with different radial clearances are compared in Figure 11. Figure 12 compares the central and minimum film thicknesses and the maximum pressure of CoC, CoM and MoM THRs, predicted from transient EHL models.

4. Discussion

The profiles of the dry contact pressure of CoM THRs investigated in the present study showed typical characteristics of hard-on-hard hip bearings. As shown in

Figures 4 and 5, the maximum pressure was at the centre of the contact area; and the pressure distribution closely resembled the Hertz contact distribution. Moreover, for all the cases solved in the present study, the differences in the maximum contact pressures and contact areas predicted by Hertz contact theory and FE methods were less than 7 percent (Table 2). These characteristics are similar to spherical MoM [17] and CoC [33] total hip bearings with thick cups. It should be noted that the backing materials underneath the CoCr insert in the present study and those in the previous studies on hard-on-hard hip bearings were different. In the present study, the materials underneath the insert were titanium shell and equivalent bone. In the MoM study [17], the backing materials were cement and bone, while in the CoC study [33], the material underneath the ceramic inlay was an ultra-high molecular weight polyethylene inlay. However, similar profiles were obtained for the contact pressure of these three types of THRs. Therefore, it can be expected that for all hard-on-hard hip bearings, if the insert (cup) is thick enough, the backing material underneath the inset (cup) and the curvature associated with the ball-in-socket contact have a small effect on the contact mechanics at the bearing surfaces.

Since film pressure is almost identical to the dry contact pressure over most of the EHL conjunction, especially under a heavy load such as that considered in the steady-state EHL models of the present study, the similarity between the film pressure and the dry contact pressure is consistent with EHL theory and thus provides some support for the solutions of both the dry contact mechanics and steady-state EHL models. It is clear that the profiles and the magnitudes of the film pressures shown in Figures 6 and 7 closely resembled those of the corresponding dry contact pressures shown in Figures 4 and 5. For example, the maximum dry contact pressure for the CoM THR with the radius of 14 mm and clearance of 60 μm was 112.6 MPa, while the corresponding maximum film pressure was 112.06 MPa.

For most of the steady-state cases investigated in Figure 8, the minimum film thicknesses predicted from the present numerical solution agreed well with the H-D formula, since such a thick-cup CoM hip bearing can be approximated as a ‘semi-infinite solid’ model. However, under heavy load and smaller viscosity, differences in the minimum film thicknesses between the present numerical solution and the H-D formula became obvious. Most likely, this is because when the lubricant film is extremely thin, more mesh nodes are needed to capture the minimum film thickness of the steady-state EHL. It is also possible that the Hamrock-Dowson formula intends to produce slightly thicker minimum film thickness, as indicated in a previous study for MoM hip implants [34]. A further investigation has to involve finer meshes. However, currently, the accurate calculation of the deformation coefficients of the bearing surfaces of hip implants for a large number of nodes is still challenging due to the requirement of extremely large computational cost for FE models.

The FE solutions of dry contact mechanics (Figures 4 and 5) and full numerical analyses of steady-state (Figures 6, 7, and 9) and transient EHL (Figures 10 and 11) indicated that head radius and radial clearance are important parameters for the tribological performance of CoM THRs in terms of reducing dry and lubricated contact pressure. For given bearing materials, dry contact and film pressures are generally determined by load and contact area. For the same load, the larger the contact area, the lower the dry contact and film pressures. Increasing size of hip replacements or/and reducing clearance between the insert and head can increase the contact area between the surfaces. As shown in Figures 4 and 6 and listed in Table 2, for a fixed radial clearance of 60 μm and a load of 3000 N, increasing R_h from 14 to 18 mm resulted in a 50 percent increase in contact area. As a result, the maximum dry contact and film pressures decreased from 112.60 to 78.41 MPa and 112.06 to 78.52 MPa, respectively. For a fixed R_h of 18 mm and a load of 3000 N, reducing c from 100 to 30 μm resulted in an increase in the contact area from 95.23 to 42.23 mm^2. Correspondingly, the maximum dry contact and film pressures decreased from 110.50 to 49.34 MPa and 111.49 to 48.98 MPa (Figures 5 and 7, Table 2), respectively. Moreover, the effects of radius and radial clearance on the film pressure are also clearly shown in transient EHL analyses (Figures 10 c and 11 c).

EHL analyses indicated that head radius and radial clearance are important parameters to enhance lubricant film thickness of CoM THRs. With a given angular velocity, a larger head radius improves the effective entraining velocity, entraining more lubricant into the contact conjunction, and slightly increases the contact area, all with the overall effect of increasing the lubricant film thickness. Therefore, an increase in the central and minimum film thicknesses is observed in Figures 9 a and 10 for CoM THRs if the radius increased from 14 to 18 mm. For example, the average increases in the central and minimum film thicknesses in one walking cycle obtained from transient EHL analyses were 45 percent and 80 percent. It should be noted that although it has been recognized that the radius of head is one of the key parameters of enhancing lubrication and minimizing wear of hard-on-hard total hip bearings, to the authors' knowledge, no full numerical analyses of the effect of radius on the lubrication performance of hard-on-hard total hip bearings have been published. Therefore, the full numerical solutions presented in Figures 9 a and 10 are also able to provide theoretical supports for other types of hard-on-hard hip bearing.

A smaller clearance produces a more conforming geometry. Such a conforming geometry reduces the pressure gradient at the inlet, resulting in the reduction in the Poiseuille flow and an increase in the Couette flow. As a result, more lubricant is allowed to flow into the loaded area to improve lubrication [35]. Therefore, a decrease in radial clearance from 100 to 30 µm caused the increase of film thickness (Figures 9 b and 11). The average increases in central and minimum film thicknesses in one walking cycle obtained from transient EHL analyses were twofold and threefold, respectively (Figure 11). This conclusion of the effect of the radial clearance on the lubrication performance of CoM hip bearings obtained from the present full numerical analyses was consistent with a previous study for general hard-on-head bearings based on the H-D formula [32].

The predictions of the effects of radius and radial clearance on the lubrication performance of CoM THRs made in the present study can be validated by published wear test results. Wear and lubrication are closely linked from a tribological point of view. An effective lubricant film is able to reduce wear significantly, while severe wear may occur if the lubricant film is not thick enough to separate the bearing surfaces. It has been shown that with similar or larger average radial clearances, 36-mm-diameter CoM bearings generated significantly lower volumetric loss than 32-mm-diameter CoM bearings [11, 12]. It has also been reported that the wear rate of 38-mm-diameter CoM bearings demonstrated lower wear rate than 32-mm-diameter CoM bearings, even though radial clearance of 38-mm-diameter CoM bearings was larger [13]. These results were all consistent with the effect of head radius on the lubrication performance of CoM THRs predicted in the present study. A smaller radial clearance producing increased film thickness agreed well with a simulator wear test of

CoM bearings [36], in which small clearances showed low wear than larger clearances for 28-mm-diameter CoM bearings.

The film thickness of CoM THR was thicker than that of the CoC THR, but thinner than that of the MoM (Figure 12), as expected. Under the same walking conditions, the only factor causing differences in the film thicknesses of the three types of bearing was the material properties of the components, which generated different elastic deformation under the same load. Since the elastic modulus of alumina is larger than that of CoCr alloy, the deformation for hip bearings with ceramic components was smaller, producing a thinner lubricant film. However, it is interesting to estimate the mode of lubrication of the three types of hip prosthesis. The estimation is usually based on the lambda ratio, which can be defined as:

$$\lambda = \frac{h_{\mathrm{min}}}{\sqrt{R_{\mathrm{a(head)}}^2 + R_{\mathrm{a(cup)}}^2}} \tag{10}$$

where h_{min} is the minimum film thickness during a walking cycle; $R_{\mathrm{a(head)}}$ and $R_{\mathrm{a(cup)}}$ are average roughnesses of the head and cup/insert respectively. In the present study, 4 nm for ceramic surface roughness and 10 nm for CoCr surface roughness were adopted [7], resulting in composite roughnesses of 5.66, 10.78 and 14.14 nm for CoC, CoM and MoM bearings, respectively. As shown in Figure 12, with similar structure and geometry, the CoC THR may operate in fluid film lubrication during the whole walking gait; the CoM THR benefited fluid film lubrication during 80 percent of a walking cycle; but the MoM THR only operated in fluid film lubrication during 30 percent of a walking cycle. Such an improvement of lubrication mode in CoM hip bearing may contribute to the reduction of metallic wear and friction of CoM hip bearings, compared with MoM hip bearings [5-9].

There are a few limitations in the present study. For example, the roughness of the bearing surfaces, which plays an important role in the lubrication and wear of hip bearings, was not considered in the EHL solution. Moreover, only steady-state and normal walking conditions were considered in the present study. However, under adverse conditions such as start-up and stopping of walking, the lubrication performance and wear of hip bearings could be significantly different from normal walking. It should also be pointed out that the mechanism for the reduced wear of the CoM hip bearings is complicated. Besides the improvement of lubrication, other factors of CoM hip bearings, such as the improvement of hardness, differential hardness reducing adhesive wear [8], and reduction in corrosive wear [37] may also contribute to the lower wear of this novel hip bearing. Furthermore, an enhancement of fluid lubrication may also help in establishment of an effective nano boundary layer on the surface of the metal [38].

5. Conclusion

For the first time, the dry contact mechanics, steady-state and transient EHL of CoM hip bearings were solved using full numerical methods. Typical dry contact and film pressure distributions and film profiles were predicted for CoM THRs. The effects of the geometric parameters, R_2 and c, on lubricated and unlubricated pressure distributions and steady-state and transient fluid film thicknesses were analyzed. The lubrication performance of CoM hip bearing was compared with that of CoC and MoM hip bearings. The following conclusions can be drawn from this study:

(1) The profiles of the dry and lubricated contact pressures of CoM THRs showed typical characteristics of hard-on-hard hip bearings: the maximum

pressure was at the centre of the contact area; the pressure distribution closely resembled the Hertz contact distribution.

(2) Full numerical analyses of contact mechanics and EHL models indicated that head radius and radial clearance are important parameters in the contact mechanics and EHL of CoM THRs. Increasing head radius and reducing radial clearance reduced contact pressure and enhanced lubricant film.

(3) The effects of head radius and radial clearance on lubrication performance were consistent with wear tests of CoM hip bearings reported in the literature.

(4) The film thickness of CoM hip bearing was thicker than that of the CoC hip bearing, but thinner than that of the MoM hip bearing. However, CoC and CoM hip bearings are more likely to benefit full fluid film lubrication than MoM hip bearings.

6. Acknowledgement

This work was supported by EPSRC and partly supported by the NIHR (National Institute for Health Research) as part of collaboration with the LMBRU (Leeds Musculoskeletal Biomedical Research Unit). JF is an NIHR Senior Fellow.

Conflict of interest statement

JF is a consultant to DePuy, the manufacturer of CoM MoM and CoC bearings. The University of Leeds and JF receive royalty income from DePuy arising from the transfer of intellectual property on bearing technology.

References:

1. Brown C, Fisher J, Ingham E. Biological effects of clinically relevant wear particles from metal-on-metal hip prostheses. Proceedings of the Institution of Mechanical Engineers, Part H: Journal of Engineering in Medicine 2006; 220(H2): 355-369.

2. Crawford R, Ranawat CS, Rothman RH. Metal on Metal: Is It Worth the Risk? Journal of Arthroplasty 2010; 25(1): 1-2.

3. Haddad FS, Thakrar RR, Hart AJ, Skinner JA, Nargol AVF, Nolan JF, et al. Metal-on-metal bearings THE EVIDENCE SO FAR. Journal of Bone and Joint Surgery-British Volume 2011; 93B(5): 572-579.

4. Langton DJ, Joyce TJ, Jameson SS, Lord J, Van Orsouw M, Holland JP, et al. Adverse reaction to metal debris following hip resurfacing - The influence of component type, orientation and volumetric wear. Journal of Bone and Joint Surgery-British Volume 2011; 93B(2): 164-171.

5. Firkins PJ, Tipper JL, Ingham E, Stone MH, Farrar R, Fisher J. A novel low wearing differential hardness, ceramic-on-metal hip joint prosthesis. Journal of Biomechanics 2001; 34(10): 1291-1298.

6. Williams S, Schepers A, Isaac G, Hardaker C, Ingham E, van der Jagt D, et al. The 2007 Otto Aufranc Award. Ceramic-on-metal hip arthroplasties: a comparative in vitro and in vivo study. Clinical Orthopaedics and Related Research 2007; 465: 23-32.

7. Brockett C, Williams S, Jin ZM, Isaac G, Fisher J. Friction of total hip replacements with different bearings and loading conditions. Journal of Biomedical Materials Research Part B-Applied Biomaterials 2007; 81B(2): 508-515.

8. Barnes CL, DeBoer D, Corpe RS, Nambu S, Carroll M, Timmerman I. Wear performance of large-diameter differential-hardness hip bearings. Journal of Arthroplasty 2008; 23(6): 56-60.

9. Bishop NE, Waldow F, Morlock MM. Friction moments of large metal-on-metal hip joint bearings and other modern designs. Medical Engineering & Physics 2008; 30(8): 1057-1064.

10. Isaac GH, Brockett C, Breckon A, van der Jagt D, Williams S, Hardaker C, et al. Ceramic-on-metal bearings in total hip replacement - Whole blood metal ion levels and analysis of retrieved components. Journal of Bone and Joint Surgery-British Volume 2009; 91B(9): 1134-1141.

11. Affatato S, Spinelli M, Squarzoni S, Traina F, Toni A. Mixing and matching in ceramic-on-metal hip arthroplasty: An in-vitro hip simulator study. Journal of

Biomechanics 2009; 42(15): 2439-2446.

12. Affatato S, Spinelli M, Zavalloni M, Traina F, Carmignato S, Toni A. Ceramic-On-Metal for Total Hip Replacement: Mixing and Matching Can Lead to High Wear. Artificial Organs 2010; 34(4): 319-323.

13. Ishida T, Clarke IC, Donaldson TK, Shirasu H, Shishido T, Yamamoto K. Comparing Ceramic-Metal to Metal-Metal Total Hip Replacements-A Simulator Study of Metal Wear and Ion Release in 32-and 38-mm Bearings. Journal of Biomedical Materials Research Part B-Applied Biomaterials 2009; 91B(2): 887-896.

14. FDA approves first ceramic-on-metal total hip replacement system. [updated 06/14/2011 cited 10/16/2011]; Available from: http://www.fda.gov/NewsEvents/Newsroom/PressAnnouncements/ucm259061.htm.

15. Dowson D. New joints for the Millennium: wear control in total replacement hip joints. Proceedings of the Institution of Mechanical Engineers Part H-Journal of Engineering in Medicine 2001; 215(H4): 335-358.

16. Williams SR, Wu JJ, Unsworth A, Khan I. Tribological and surface analysis of 38 mm alumina-as-cast Co-Cr-Mo total hip arthroplasties. Proceedings of the Institution of Mechanical Engineers Part H-Journal of Engineering in Medicine 2009; 223(H8): 941-954.

17. Jagatia M, Jin ZM. Elastohydrodynamic lubrication analysis of metal-on-metal hip prostheses under steady state entraining motion. Proceedings of the Institution of Mechanical Engineers Part H-Journal of Engineering in Medicine 2001; 215(H6): 531-541.

18. Wang FC, Jin ZM. Transient elastohydrodynamic lubrication of hip joint implants. Journal of Tribology-Transactions of the ASME 2008; 130(1): 011007.

19. Bergmann G, Deuretzbacher G, Heller M, Graichen F, Rohlmann A, Strauss J, et al. Hip contact forces and gait patterns from routine activities. Journal of Biomechanics 2001; 34(7): 859-871.

20. Jin ZM. Theoretical studies of elastohydrodynamic lubrication of artificial hip joints. Proceedings of the Institution of Mechanical Engineers, Part J: Journal of Engineering Tribology 2006; 220(J8): 719-727.

21. ISO 14242-1, Implants for Surgery - Wear of Total Hip-Joint Prostheses - Part 1: Loading and Displacement Parameters for Wear-Testing Machines and Corresponding Environmental Conditions for Test. 2002.

22. Cooke AF, Dowson D, Wright V. The rheology of synovial fluid and some potential synthetic lubricants for degenerate synovial joints. Engineering in Medicine 1978; 7: 66-72.

23. Yao JQ, Laurent MP, Johnson TS, Blanchard CR, Crowninshield RD. The influences of lubricant and material on polymer/CoCr sliding friction. Wear 2003; 255(1-6): 780-784.

24. Wang WZ, Jin ZM, Dowson D, Hu YZ. A study of the effect of model geometry and lubricant rheology upon the elastohydrodynamic lubrication performance of metal-on-metal hip joints. Proceedings of the Institution of Mechanical Engineers Part J-Journal of Engineering Tribology 2008; 222(J3): 493-501.

25. Meng QE, Gao LM, Liu F, Yang PR, Fisher J, Jin ZM. Transient elastohydrodynamic lubrication analysis of a novel metal-on-metal hip prosthesis with an aspherical acetabular bearing surface. Journal of Medical Biomechanics 2009; 24(5): 352-362.

26. Gao L, Wang F, Yang P, Jin Z. Effect of 3D physiological loading and motion on elastohydrodynamic lubrication of metal-on-metal total hip replacements. Medical Engineering & Physics 2009; 31(6): 720-729.

27. Gao LM, Meng QE, Wang FC, Yang PR, Jin ZM. Comparison of numerical methods for elastohydrodynamic lubrication analysis of metal-on-metal hip implants: multi-grid verses Newton-Raphson. Proceedings of the Institution of Mechanical Engineers, Part J: Journal of Engineering Tribology 2007; 221(J2): 133-140.

28. Venner CH, Multigrid solution of the EHL line and point contact problems. PhD Thesis. 1991, Enschede: University of Twente.

29. Liu F, Jin ZM, Hirt F, Rieker C, Roberts P, Grigoris P. Transient elastohydrodynamic lubrication analysis of metal-on-metal hip implant under simulated walking conditions. Journal of Biomechanics 2006 a; 39(5): 905-914.

30. Wang FC, Jin ZM. Prediction of elastic deformation of acetabular cups and femoral heads for lubrication analysis of artificial hip joints. Proceedings of the Institution of Mechanical Engineers Part J-Journal of Engineering Tribology 2004 a; 218(J3): 201-209.

31. Hamrock BJ, Dowson D. Elastohydrodynamic lubrication of elliptical contacts for materials of low elastic-modulus. I: Fully flooded conjunction. Journal of Lubrication Technology-Transactions of the ASME 1978; 100(2): 236-245.

32. Jin ZM, Dowson D, Fisher J. Analysis of fluid film lubrication in artificial hip joint replacements with surfaces of high elastic modulus. Proceedings of the Institution of Mechanical Engineers Part H-Journal of Engineering in Medicine 1997; 211(3): 247-256.

33. Mak MM, Jin ZM. Analysis of contact mechanics in ceramic-on-ceramic hip joint replacements. Proceedings of the Institution of Mechanical Engineers

Part H-Journal of Engineering in Medicine 2002; 216(H4): 231-236.

34. Jalali-Vahid D, Jin ZM, Dowson D. Isoviscous elastohydrodynamic lubrication of circular point contacts with particular reference to metal-on-metal hip implants. Proceedings of the Institution of Mechanical Engineers Part J-Journal of Engineering Tribology 2003; 217(J5): 397-402.

35. Meng QE, Liu F, Fisher J, Jin ZM. Transient elastohydrodynamic lubrication analysis of a novel metal-on-metal hip prosthesis with a non-spherical femoral bearing surface. Proceedings of the Institution of Mechanical Engineers Part H-Journal of Engineering in Medicine 2011; 225(H1): 25-37.

36. Haider H, Weisenburger JN, Naylor MG, Schroeder DW, Croson RE, Garvin KL. Bearing diameter, radial clearance and their effect on wear in ceramic-on-metal total hip replacements. In 54th Annual Meeting of the Orthopaedic Research Society. 2008. San Francisco, California, USA. Poster 1792.

37. Figueiredo-Pina CG, Yan Y, Neville A, Fisher J. Understanding the differences between the wear of metal-on-metal and ceramic-on-metal total hip replacements. Proceedings of the Institution of Mechanical Engineers Part H-Journal of Engineering in Medicine 2008; 222(H3): 285-296.

38. Pourzal R, Theissmann R, Williams S, Gleising B, Fisher J, Fischer A. Subsurface changes of a MoM hip implant below different contact zones. Journal of the Mechanical Behavior of Biomedical Materials 2009; 2(2): 186-191.

Nomenclature:

c	radial clearance between head and insert
e_x, e_y	eccentricity components of the femoral head in x and y directions
E_c, E_h	elastic moduli of insert and head, respectively
E'	equivalent elastic modulus of bearing surfaces
f_x, f_y, f_z	calculated load components
h	film thickness
h_{min}	the minimum film thickness
p	pressure
r	contact radius calculated from Hertz contact theory
R	radius of the equivalent ball of the equivalent ball-on-plane model
$R_{a(cup)}$	average roughness of the insert
$R_{a(head)}$	average roughness of the head
R_h	radius of femoral head
R_c	radius of the cup/insert
t	time (s)
u	effective entraining velocity
w_y	applied load in y direction
x, y, z	Cartesian coordinates
δ	elastic deformation the femoral head and acetabular cup
η	viscosity of synovial fluid
ϕ, θ	angular coordinates in the entraining and side-leakage directions respectively.
λ	lambda ratio
ν_c, ν_h	Poison's rations of insert and head, respectively
ω	angular velocity

Captions

Table 1 Material properties used for CoCr alloy, titanium, alumina and equivalent support layer

Table 2 Comparison of the predicted maximum contact pressure and contact area between the present finite element study and the Hertz contact theory

Figure 1 A ball-in-socket configuration for contact mechanics and EHL analyses of CoM bearings

Figure 2 Variation in the load (a) and velocity (b) of the walking conditions based on ISO 14242-1

Figure 3 Definition of spherical coordinates and mesh grid

Figure 4 Contour plots of dry contact pressure (MPa) at the bearing surface of CoM hip replacements with a similar radial clearance (60 µm) but different radii: (a) 14 mm, (b) 16 mm, (c) 18 mm

Figure 5 Contour plots of dry contact pressure (MPa) at the bearing surface of CoM hip replacements with a similar radius (18 mm) but different radial clearances: (a) 100 µm, (b) 30 µm

Figure 6 Contour plots of steady-state film pressure (MPa) in CoM hip replacements with similar radial clearance (60 µm) but different radii: (a) 14 mm, (b) 16 mm, (c) 18 mm

Figure 7 Contour plots of steady-state film pressure (MPa) in CoM hip replacements with similar radius (18 mm) but different radial clearances: (a) 100 µm, (b) 30 µm

Figure 8 Minimum film thicknesses produced by the H-D formula and current numerical model for a 36-mm-diameter CoM THR with radial clearance of 60 µm under different loads

Figure 9 Comparison of steady-state film thickness on the central line along the entraining direction for different radii (c = 60 µm) (a) and radial clearances (R_h = 18 mm) (b)

Figure 10 Prediction of the central film thickness (a), minimum film thickness (b) and maximum pressure (c) by transient EHL solution for CoM hip replacements with a similar radial clearance (60 µm) but different radii, under transient conditions based on ISO 14242-1

Figure 11 Prediction of the central film thickness (a), minimum film thickness (b) and maximum pressure (c) by transient EHL solution for CoM hip replacements with a similar size (18 mm) but different radial clearances, under transient conditions based on ISO 14242-1

Figure 12 Under transient conditions based on ISO 14242-1, prediction of the central film thickness (a), minimum film thickness (b) and maximum pressure (c) by transient EHL solution for CoM, CoC and MoM hip replacements with similar size (18 mm) and radial clearance (60 μm)

Table 1 Material properties used for CoCr alloy, titanium, alumina and equivalent support layer

	Elastic modulus (GPa)	Poisson's ratio
CoCr	210	0.3
Titanium	110	0.3
Equivalent support layer	2.27	0.23
Alumina	380	0.26

Table 2 Comparison of the predicted maximum contact pressure and contact area between the present finite element study and the Hertz contact theory

Radius (mm)	Radial clearance (μm)	Maximum contact pressure (MPa)		Contact area (mm^2)	
		Finite element	Hertz	Finite element	Hertz
14	60	112.60	105.40	40.51	42.69
16	60	92.89	88.24	48.52	50.99
18	60	78.41	75.44	61.35	59.65
18	30	49.34	47.58	95.29	94.58
18	100	110.50	105.89	42.23	42.50

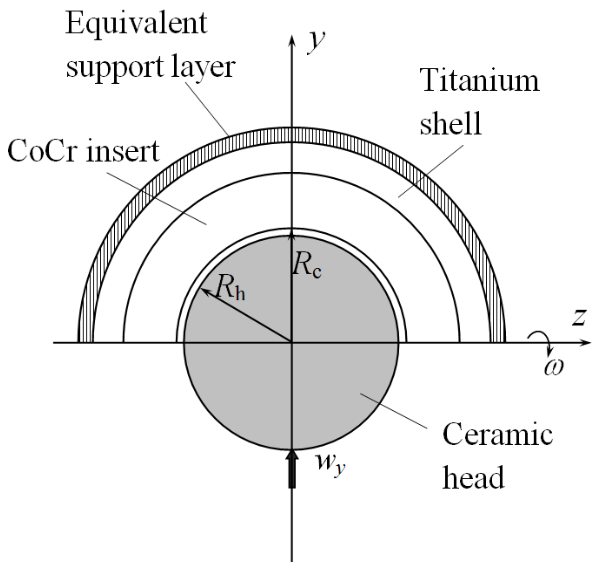

Figure 1 A ball-in-socket configuration for contact mechanics and EHL analyses of CoM bearings

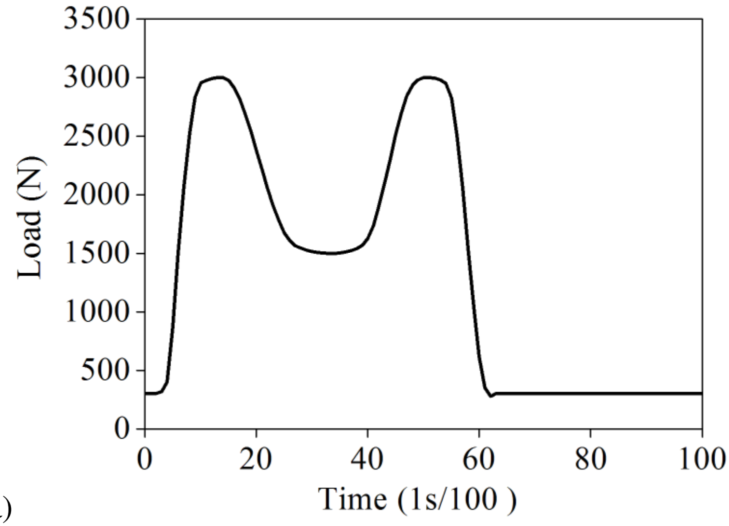

(a)

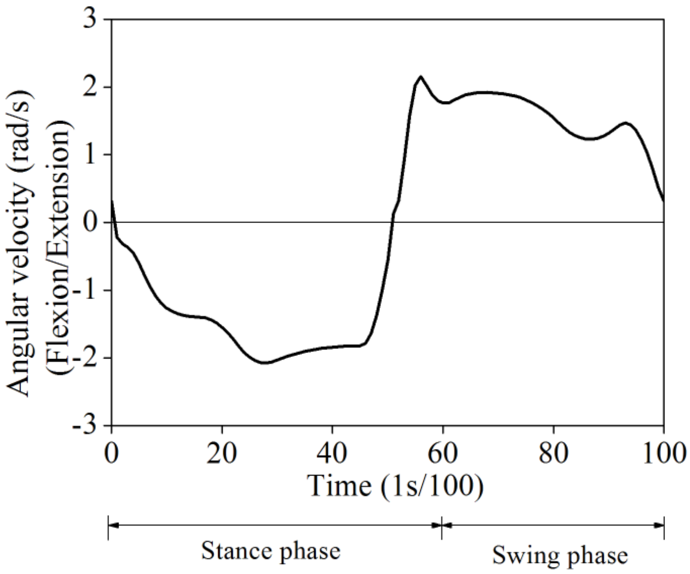

(b)

Figure 2 Variation in the load (a) and velocity (b) of the walking conditions based on ISO 14242-1

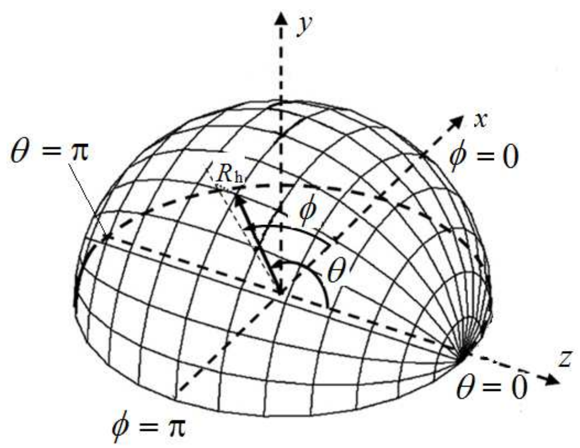

Figure 3 Definition of spherical coordinates and spherical mesh grid

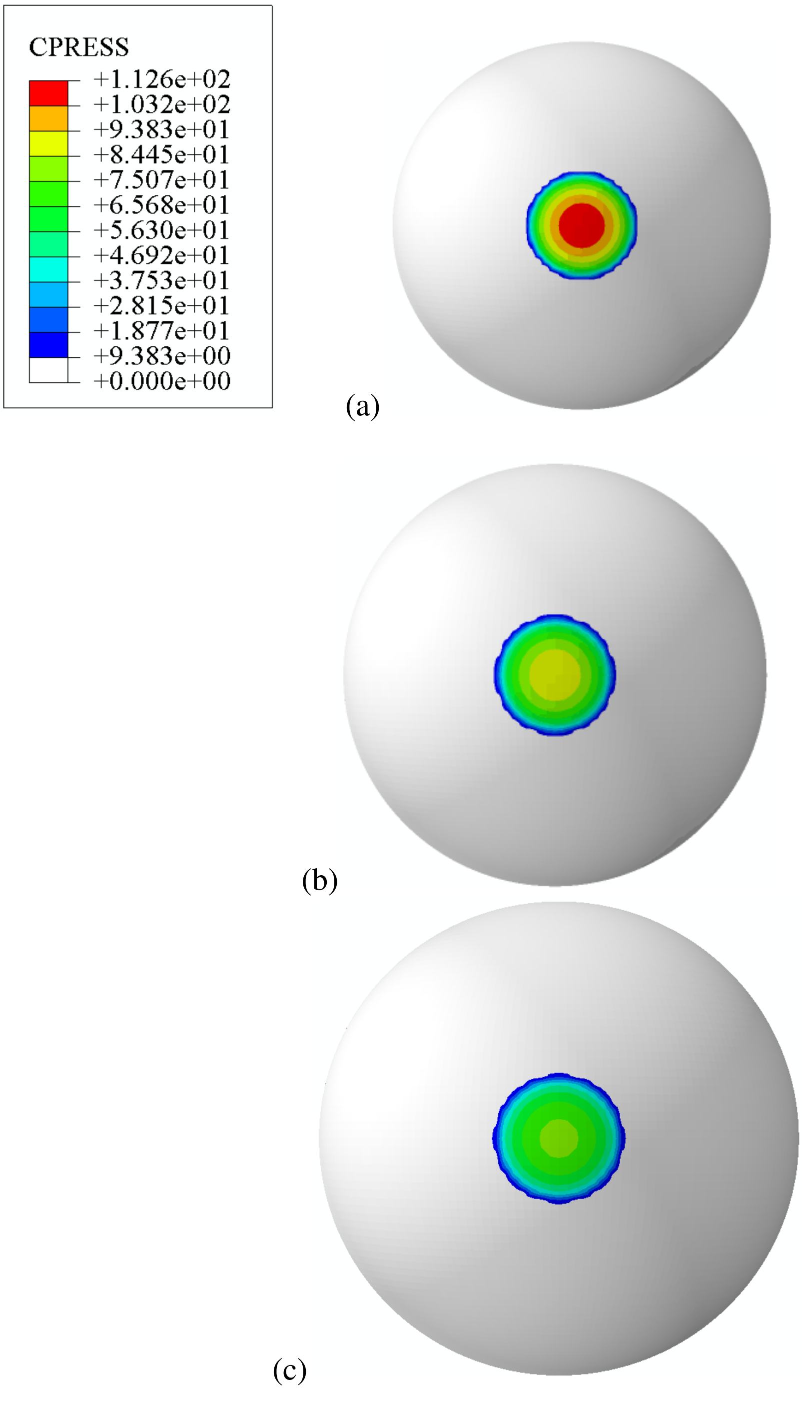

Figure 4 Contour plots of dry contact pressure (MPa) at the bearing surface of CoM hip replacements with a similar radial clearance (60 μm) but different radii: (a) 14 mm, (b) 16 mm, (c) 18 mm

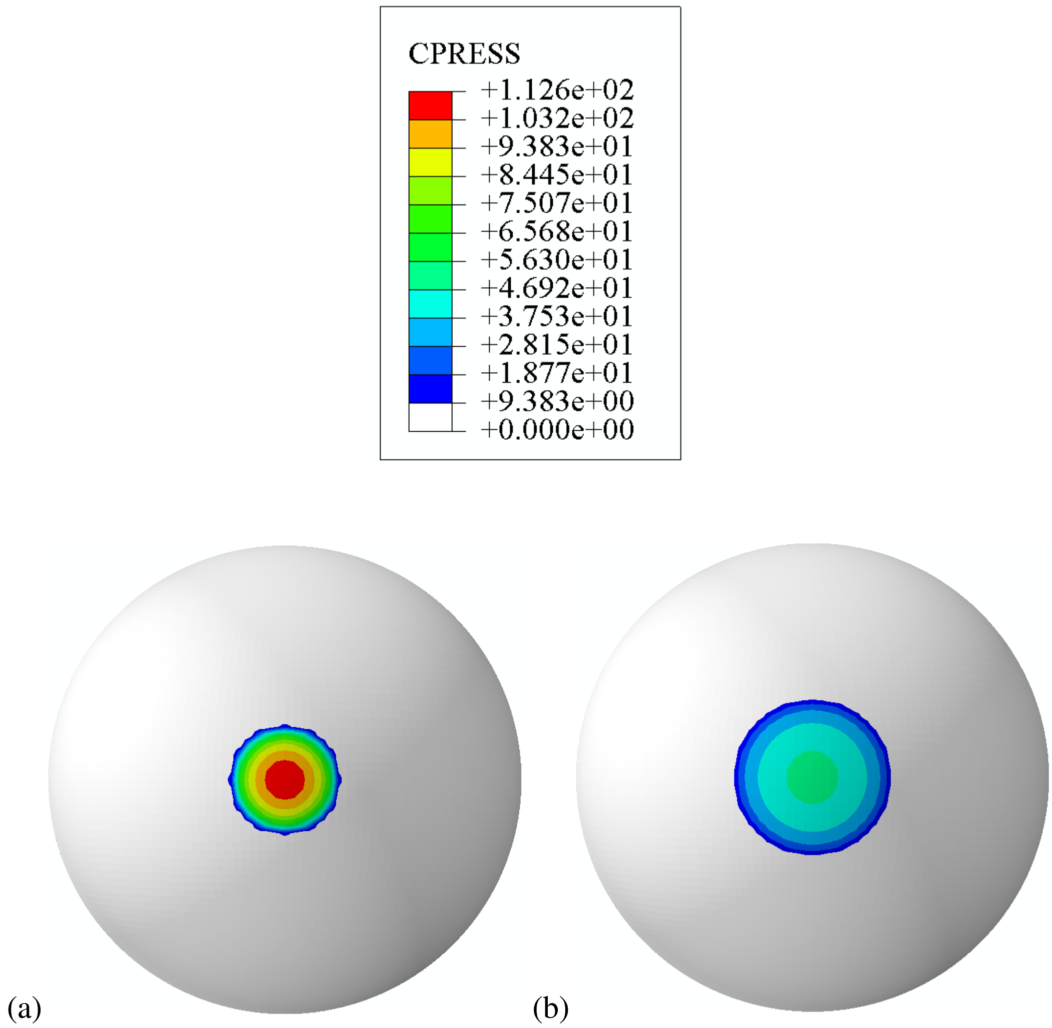

Figure 5 Contour plots of dry contact pressure (MPa) at the bearing surface of CoM hip replacements with a similar radius (18 mm) but different radial clearances: (a) 100 μm, (b) 30 μm

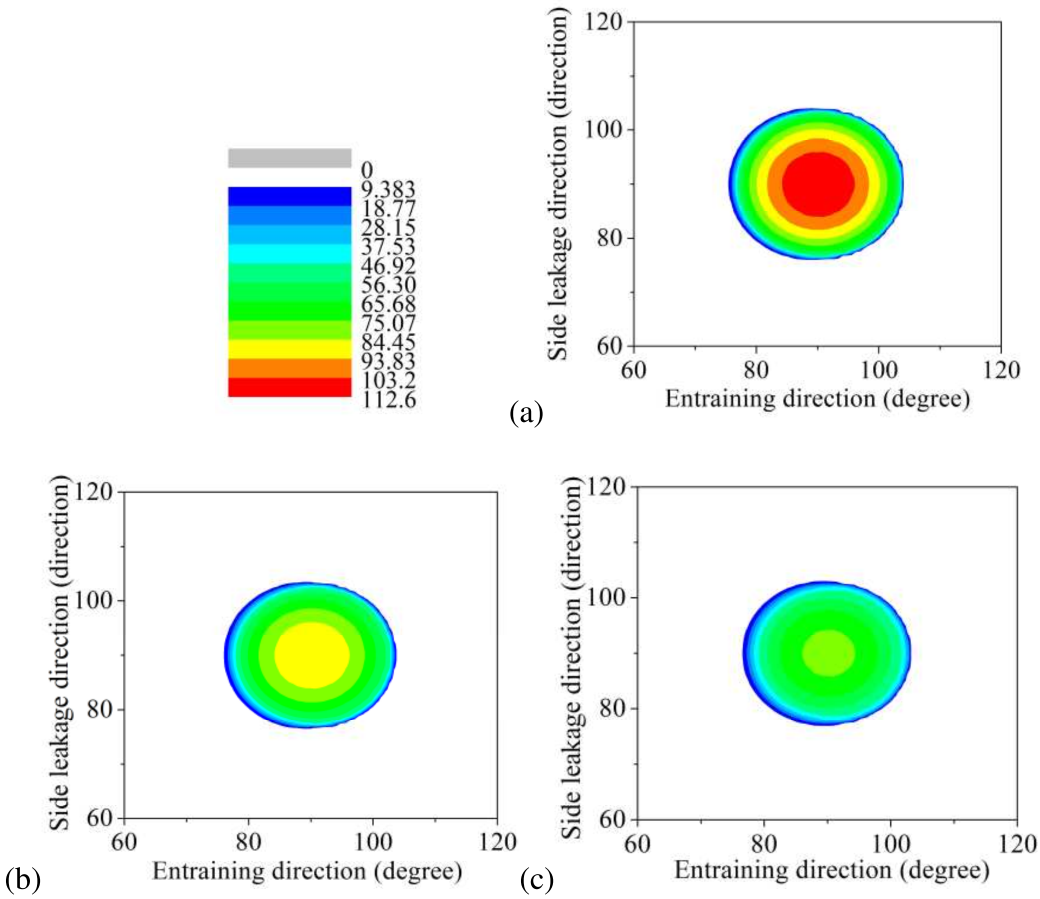

Figure 6 Contour plots of steady-state film pressure (MPa) in CoM hip replacements with similar radial clearance (60 μm) but different radii: (a) 14 mm, (b) 16 mm, (c) 18 mm

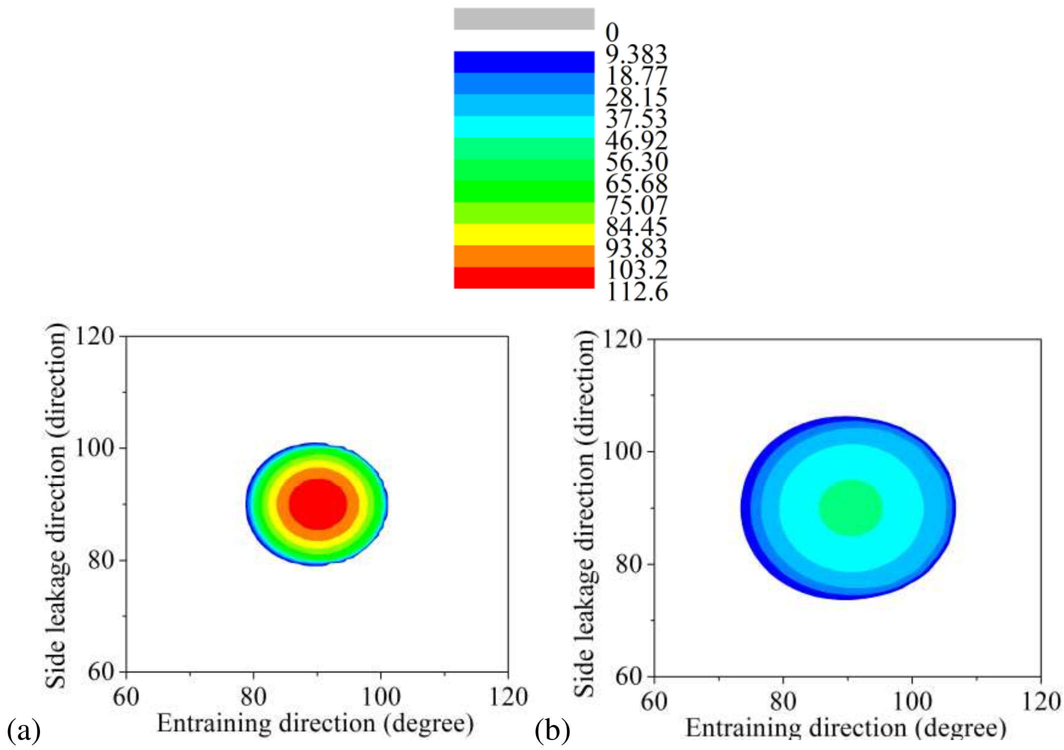

Figure 7 Contour plots of steady-state film pressure (MPa) in CoM hip replacements with similar radius (18 mm) but different radial clearances: (a) 100 μm, (b) 30 μm

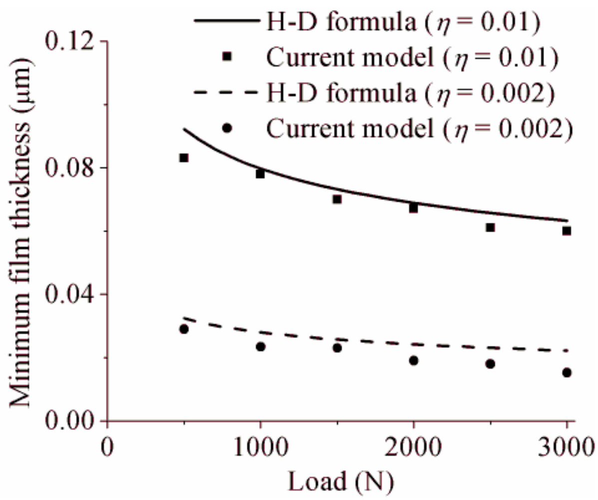

Figure 8 Minimum film thicknesses produced by the H-D formula and current numerical model under different loads for a 36-mm-diameter CoM THR with radial clearance of 60 μm

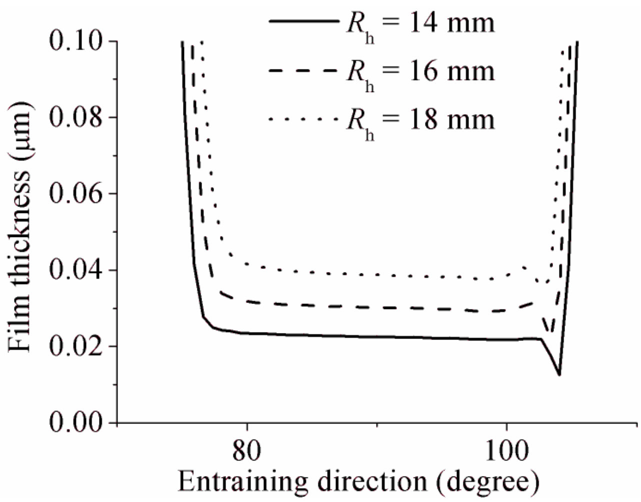

(a)

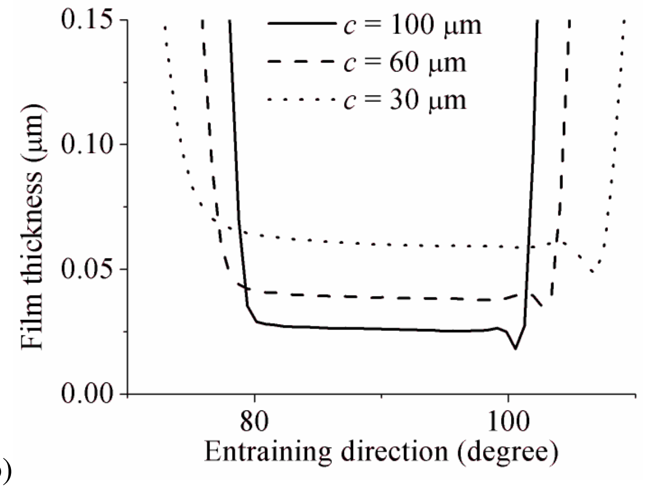

(b)

Figure 9 Comparison of steady-state film thickness on the central line along the entraining direction for different radii (c = 60 μm) (a) and radial clearances (R_h = 18 mm) (b)

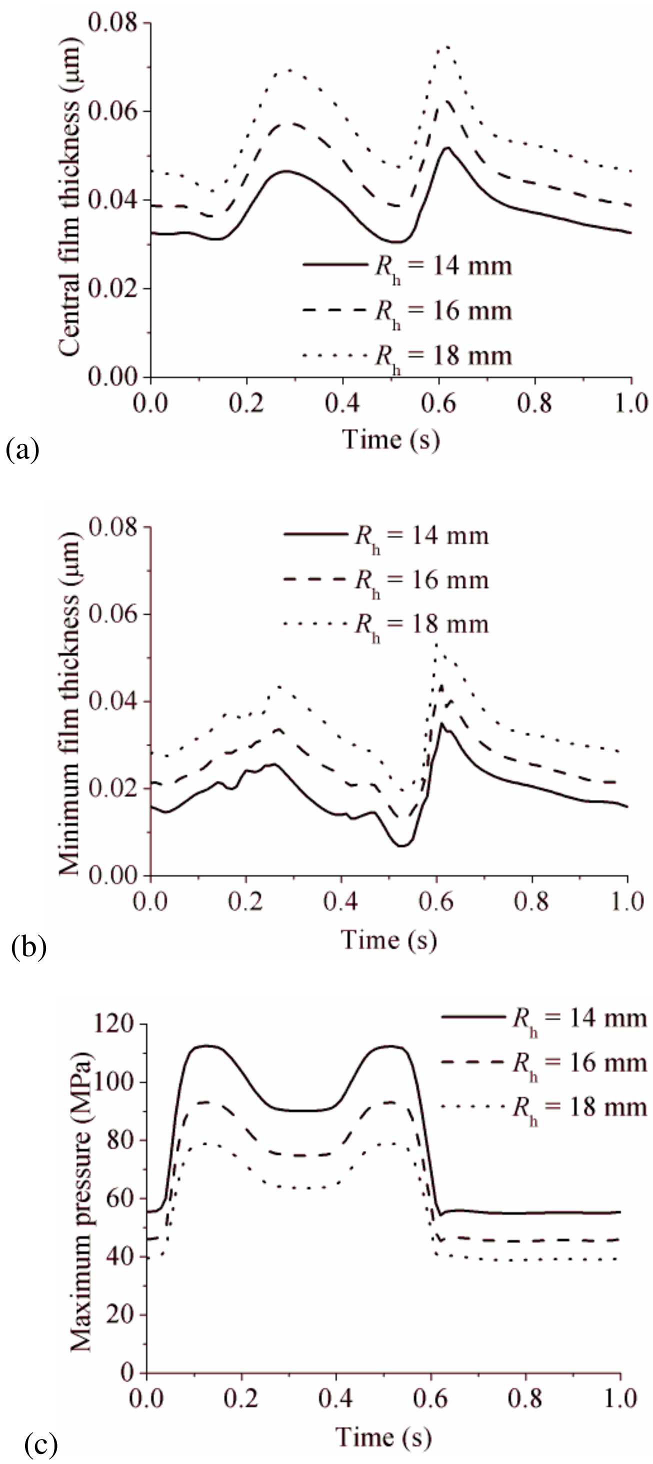

Figure 10 Prediction of the central film thickness (a), minimum film thickness (b) and maximum pressure (c) by transient EHL solution for CoM hip replacements with a similar radial clearance (60 μm) but different radii, under transient conditions based on ISO 14242-1

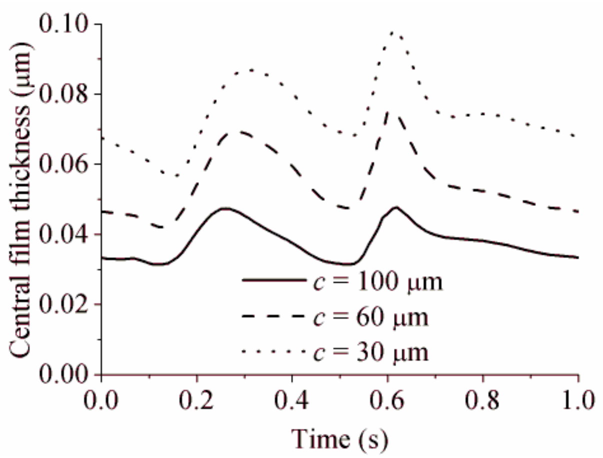

(a)

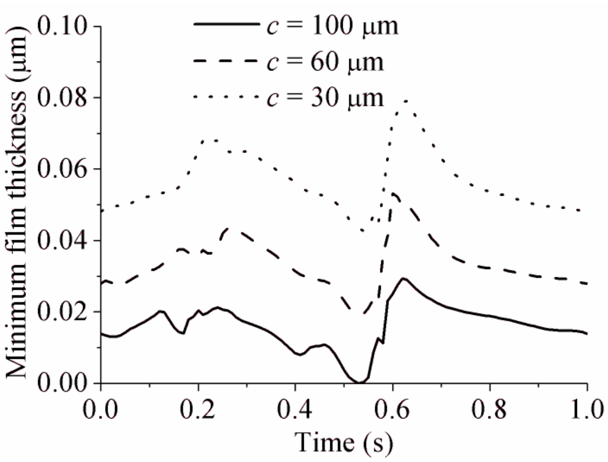

(b)

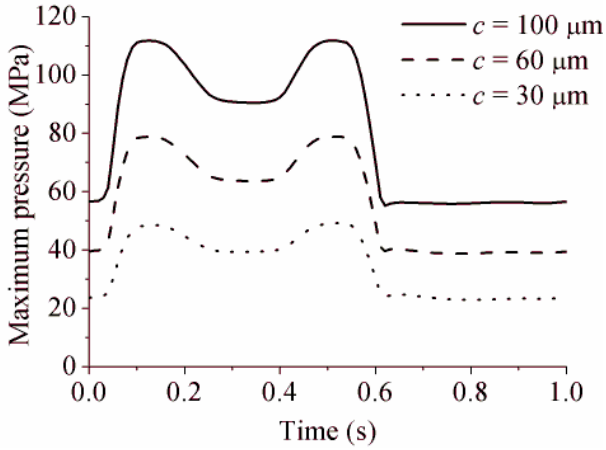

(c)

Figure 11 Prediction of the central film thickness (a), minimum film thickness (b) and maximum pressure (c) by transient EHL solution for CoM hip replacements with a similar size (18 mm) but different radial clearances, under transient conditions based on ISO 14242-1

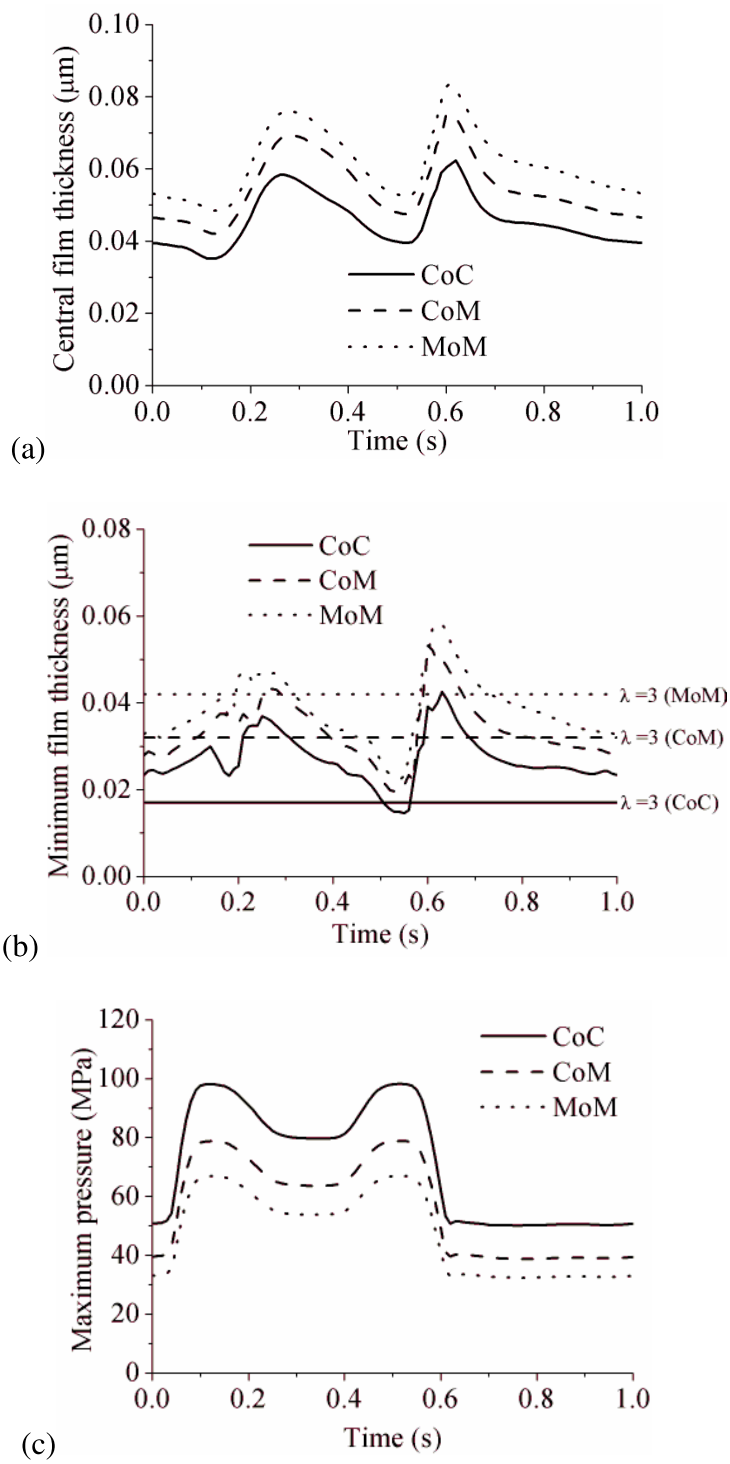

Figure 12 Under transient conditions based on ISO 14242-1, prediction of the central film thickness (a), minimum film thickness (b) and maximum pressure (c) by transient EHL solution for CoM, CoC and MoM hip replacements with similar size (18 mm) and radial clearance (60 μm)